


Preparation of Graphene–Zinc Oxide Nanostructure Composite for Carbon Monoxide Gas Sensing

AHMAD RIFQI MUCHTAR,¹ NI LUH WULAN SEPTIANI,¹
MUHAMMAD IQBAL,¹ AHMAD NURUDDIN,¹
and BRIAN YULIARTO ^{1,2,3}

1.—Advanced Functional Materials Laboratory, Engineering Physics Department, Faculty of Industrial Technology, Institut Teknologi Bandung, Bandung, Indonesia. 2.—Research Center for Nanosciences and Nanotechnology, Institut Teknologi Bandung, Bandung, Indonesia. 3.—e-mail: brian@tf.itb.ac.id

A simple method to synthesize graphene–zinc oxide nanocomposite has been developed. A reduced graphene oxide–ZnO nanocomposite was prepared using a reflux method with ethylene glycol as medium. X-ray diffraction analysis, scanning electron microscopy, energy-dispersive spectrometry, and nitrogen adsorption–desorption measurements were used to characterize the resulting composite materials. The highest response of about 98% was observed when using pure ZnO at 300°C, while the second highest sensor response of about 96% was achieved by graphene–ZnO with 1:3 composition. It was found that the graphene–zinc oxide hybrid has potential to improve sensor performance at low temperature. The graphene–ZnO hybrid with 1:3 composition showed good response of 36% at 125°C, an operating temperature at which pure ZnO showed no response.

Key words: Reduced graphene oxide, zinc oxide, nanostructured material, composite, gas sensor, carbon monoxide

INTRODUCTION

Improving air quality and mitigating air pollution have become a major mission worldwide. Air pollution is actually a heterogeneous mixture of gases and particulate matter.¹ The main gaseous components of air pollution are ozone, carbon monoxide (CO), nitrogen dioxide, and sulfur dioxide.¹ CO gas is an odorless, colorless, and tasteless air toxin that can be poisonous to humans. CO gas can be produced by incomplete combustion of hydrocarbons. The most significant emission sources of CO gas are motor vehicles, tobacco smoke, heating systems, portable generators, and gas stoves.² Consequently, CO gas is a common contaminant of both outdoor and indoor environments.³ Exposure to CO gas may cause headache, dizziness, vomiting, and

nausea. In fact, all people are at risk of poisoning by CO gas, but unborn babies, infants, the elderly, and people with chronic heart disease, anemia, or respiratory problems are generally more at risk than others. Given these dangers, it is urgently necessary to enable accurate monitoring of CO concentrations. CO gas monitoring systems need sensors and data acquisition systems that can detect presence of CO gas at any concentration. Moreover, high-performance CO sensors that increase the accuracy and reliability of such monitors are highly sought after.

One potential application of graphene is detection of gaseous molecules, enabling its use in gas sensing applications. Graphene's high surface area to mass ratio, high electrical conductivity, and ability to work at room temperature represent advantages that could be utilized in gas sensing. Presence of a gas molecule on the surface of graphene causes the molecule to be adsorbed, resulting in electron conductance. The gas molecule can be an electron donor or acceptor, changing the amount or mobility of charge carriers in graphene.⁴ While it has been

shown that graphene can detect small amounts of gas, indeed even a single molecule,⁵ it lacks the ability to detect larger amounts of gas at ppm scale. Variation of the composition as well as doping of graphene onto existing sensing materials are believed to be appropriate approaches to improve the detection range in terms of sensitivity and selectivity.

Zinc oxide (ZnO) has already proved to be able to detect gas molecules with high sensitivity. It has a wide bandgap and many point defects on which physisorption and chemisorption occur.⁶ ZnO can be synthesized as many nanoscale structures, such as nanoparticles, nanorods, and nanosheets, which offer increased surface area and hence increased sensor sensitivity and selectivity.^{7–9} However, for gas sensing applications, ZnO requires high operating temperature of 250°C to 400°C to achieve optimum sensitivity and enhance the surface molecular desorption kinetics for faster recovery time. As a result, such sensors require high power to achieve their full potential and, in many cases, still show slow recovery time. The future will see avoidance of high-temperature operation for metal oxide devices in many applications, because electrical devices should offer low power consumption for environmental reasons.

Many experiments have already demonstrated the role of graphene when doped into metal oxide materials for use in various applications, including gas sensing. In particular, the adsorption capacity and electron transport channels offered by graphene have led to the emergence of gas sensors with improved performance.¹⁰ For gas sensing applications, doping of graphene into a metal or metal oxide resulted in good response at relatively low temperature.^{11–15} However, to date, study of the sensing mechanism of graphene–ZnO composites has remained sparse. This paper reports a simple approach for synthesis of graphene–ZnO composite layers for gas sensing using an easy and low-cost preparation technique. The requirements for a gas sensor vary depending on its application and may include low cost, low power, high sensitivity, and fast response and recovery times. Low cost requires a simple yet effective method to form the gas sensor. In this research, graphene synthesized by the chemical exfoliation process was used, being both low cost and feasible for mass production, compared with other synthesis processes. As the aim of this work is to synthesize graphene–ZnO composites, reduced graphene oxide (rGO) was purchased from a commercial source. To synthesize the composites, a reflux method was used, being both simple and low cost. An alumina plate was used as substrate, on which the graphene–ZnO nanocomposite sensor was deposited. In this research, 30 ppm CO was chosen, as this value is commonly used in many standards as the level at which CO begins to be dangerous to human health.

EXPERIMENTAL PROCEDURES

Synthesis of Graphene–ZnO Nanocomposite

For simplicity, the rGO–ZnO composite is called GZ. rGO was obtained from Skyspring Nanomaterials Inc. Analytical-grade zinc nitrate tetrahydrate [$\text{Zn}(\text{NO}_3)_2 \cdot 4\text{H}_2\text{O}$] as ZnO precursor and ethylene glycol were obtained from Merck and used without any further purification. The rGO: $\text{Zn}(\text{NO}_3)_2 \cdot 4\text{H}_2\text{O}$ mole ratio of precursors was 3:1, 1:1, and 1:3, with the amount of rGO kept constant in each case, with 40 ml, 60 ml, and 80 ml ethylene glycol, respectively. The simple reflux system employed consisted of a flat-bottomed flask, Liebig condenser with stand, Bunsen burner with wire gauze and tripod, and minisubmersible water pump to circulate condensing water.

The reflux procedure started with mixing the precursor with ethylene glycol in the flask, followed by ultrasonication for 30 min to ensure a homogeneous mixture. After that, the mixture was refluxed at 190°C. First, pure ZnO was synthesized by observing the change in color; this reflux process took 12 h. While refluxing the three composites, the change that occurred in the mixture was difficult to observe because the rGO caused the mixture to be colored black, hence the reflux process for the three variations was also set at 12 h. After 12 h of reflux, the system was aged for 12 h for settling. The resultant was filtered then washed three times with ethanol and Aqua Bidest. The resulting material was calcined at 450°C for 2 h, finally obtaining the powder sensor materials, denoted as rGO, GZ 3:1, GZ 1:1, GZ 1:3, and ZnO.

Material Characterization

X-ray diffraction analysis (Philips Analytical, 40 kV, 30 mA, 2θ range 15° to 60° with step size of 0.020°) was used to confirm the crystal structure of the five samples. Chemical properties of the samples was analyzed using Fourier Transform Infrared Spectroscopy (FTIR) Thermoscientific Nicolet 4700. Surface morphology was characterized by scanning electron microscopy (SEM, LEO type 420i) at 100,000× magnification. Brunauer–Emmett–Teller (BET) surface area analysis was carried out by nitrogen adsorption–desorption using a Quantachrome Instruments version 11.03. Elemental composition was determined using a JEOL JED-2300 analysis station.

Sensor Fabrication

Sensor devices were prepared using a thick-film method as follows: A certain amount of powder was carefully dispersed in ethylene glycol to form a paste, which was then deposited onto the alumina substrate, on which a conductive silver paste electrode had been previously deposited. The resulting film was then dried at 200°C for 1 h. Figure 1 shows a schematic of the sensor devices, indicating the

position of the sensing film layer of graphene–ZnO nanocomposite and the electrode. Figure 2 depicts the scheme for gas sensor testing. Gas cylinders containing CO and nitrogen were connected to a mixing chamber. Bacharach PCA3 was used to confirm the concentration of CO in the mixing chamber. Until the desired ppm level was obtained, the diluted CO gas was streamed to the first bubbler. Fuji PXR-9 temperature controller and Omron G3PX-220EH power controller were used to control the desired operating temperature. Picotest M3500A was used to log the sensor resistance data to a computer.

RESULTS AND DISCUSSION

Figure 3 shows the diffraction patterns of the five samples of graphene–ZnO nanocomposite. The broad peak observed for rGO at 26.5° can be assigned to (002) plane, consistent with the typical diffraction of rGO. Another broad peak at 43° is in accordance with the graphite (100) plane, indicating a lower degree of crystallization and presence of some defects.¹⁵ The diffraction pattern of pure ZnO showed signals from (100), (002), (101), (102), and (110) planes of wurtzite crystal structure, matching well with Joint Committee on Powder Diffraction

Standards (JCPDS) card no. 36-1451.¹⁶ In the diffraction pattern of graphene–ZnO with 3:1 composition, the (002) plane of rGO was visible. Moreover, in graphene–ZnO with 1:1 and 1:3 compositions, no peaks for rGO were visible. This phenomenon simply indicates that, in the graphene–ZnO nanocomposite with 3:1 composition, the ZnO particles did not fully cover the rGO sheets, while in the graphene–ZnO nanocomposite with 1:1 or 1:3 composition, the ZnO particles completely covered the rGO sheets. The diffraction patterns of the three composites were also similar to that of ZnO, indicating that addition of rGO in the reflux process did not affect the formation or orientation of ZnO crystals. Furthermore, from the XRD plot, it was observed that the concentration of graphene added affected the width of the ZnO peaks. In other words, introduction of graphene into ZnO affected the crystallite size of ZnO. To investigate this effect, the crystallite size was calculated using the Scherrer formula (Eq. 1), where K is the Scherrer constant (0.9 for spherical particles), λ is the wavelength of Cu K_α radiation (1.54 Å), and B is the full-width at half-maximum intensity of the peak (Table I).¹⁷ The lattice constant was also determined using Bragg's law (Eqs. 2 and 3).¹⁷ The crystallite size of ZnO tended to increase as the concentration of graphene was increased, but decreased for G:ZnO ratio of 3:1. The lattice constants also changed in the presence of graphene. Presence of graphene can cause lattice stress and strain in ZnO.

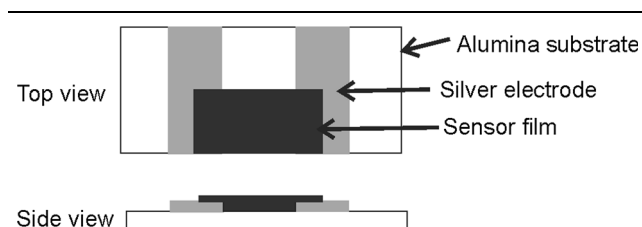


Fig. 1. Schematic of sensor device, showing electrode and deposited graphene–ZnO nanocomposite sensing film.

$$d = \frac{K\lambda}{B\cos\theta}, \quad (1)$$

$$a = \sqrt{\frac{1}{3} \frac{\lambda}{\sin\theta}}, \quad (2)$$

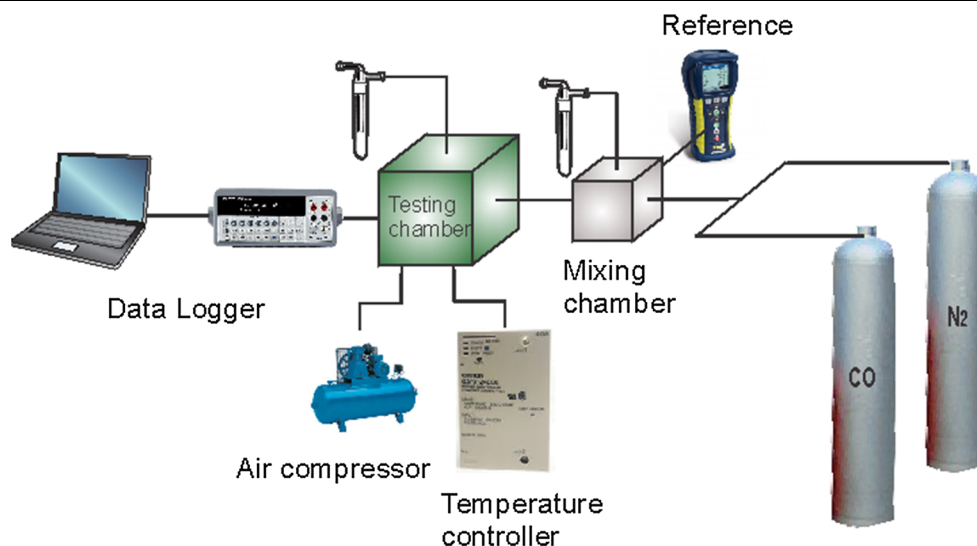


Fig. 2. Scheme of gas sensing characterization system.

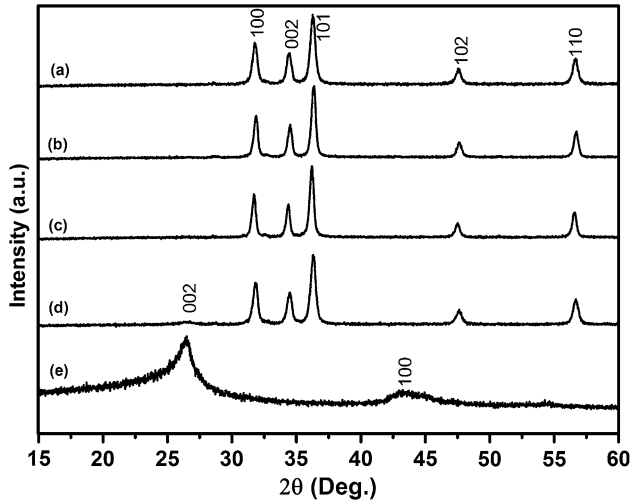


Fig. 3. X-ray diffraction results for five samples of GZ with ratio (a) 0:1, (b) 1:3, (c) 1:1, (d) 3:1, and (e) 1:0.

$$c = \frac{\lambda}{\sin\theta}. \quad (3)$$

The Fourier-transform infrared (FTIR) spectra of graphene, the G-ZnO nanocomposites, and ZnO are shown in Fig. 4. The broad peaks at 3431 cm^{-1} for graphene and G:ZnO 3:1 (Fig. 4d and e) came from O-H stretching vibration.¹⁸ This peak became smaller as the concentration of ZnO was increased, and vanished for the ZnO sample. All sample nanocomposites showed peaks at 1573 cm^{-1} and 1184 cm^{-1} , attributed to stretching vibrations of C=C and C-OH, respectively. Moreover, the additional peak at 451 cm^{-1} was attributed to ZnO.

Surface morphology analysis of all samples is shown in Fig. 5. The graphene sheets are very hard to observe in Fig. 5a and b. Graphene is a two-dimensional material with very high specific surface area. Its high surface energy makes it agglomerate

Table I. Crystallite size calculated using Scherrer formula and lattice constant calculated using Bragg's law for all samples

Sample	Crystallite size (nm)	Lattice constant, a (Å)	Lattice constant, c (Å)
G:ZnO 3:1	18	3.24	5.19
G:ZnO 1:1	23	3.25	5.20
G:ZnO 1:3	22	3.23	5.19
ZnO	20	3.24	5.20

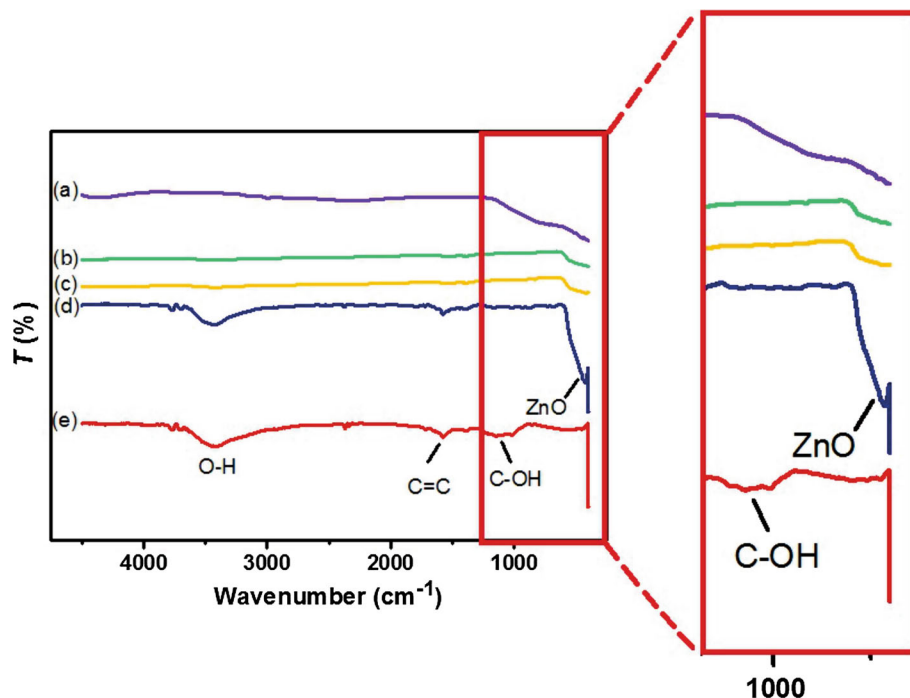


Fig. 4. (a) FTIR spectra of ZnO. GZ nanocomposites with ratios of (b) 1:3, (c) 1:1, and (d) 3:1. (e) rGO.

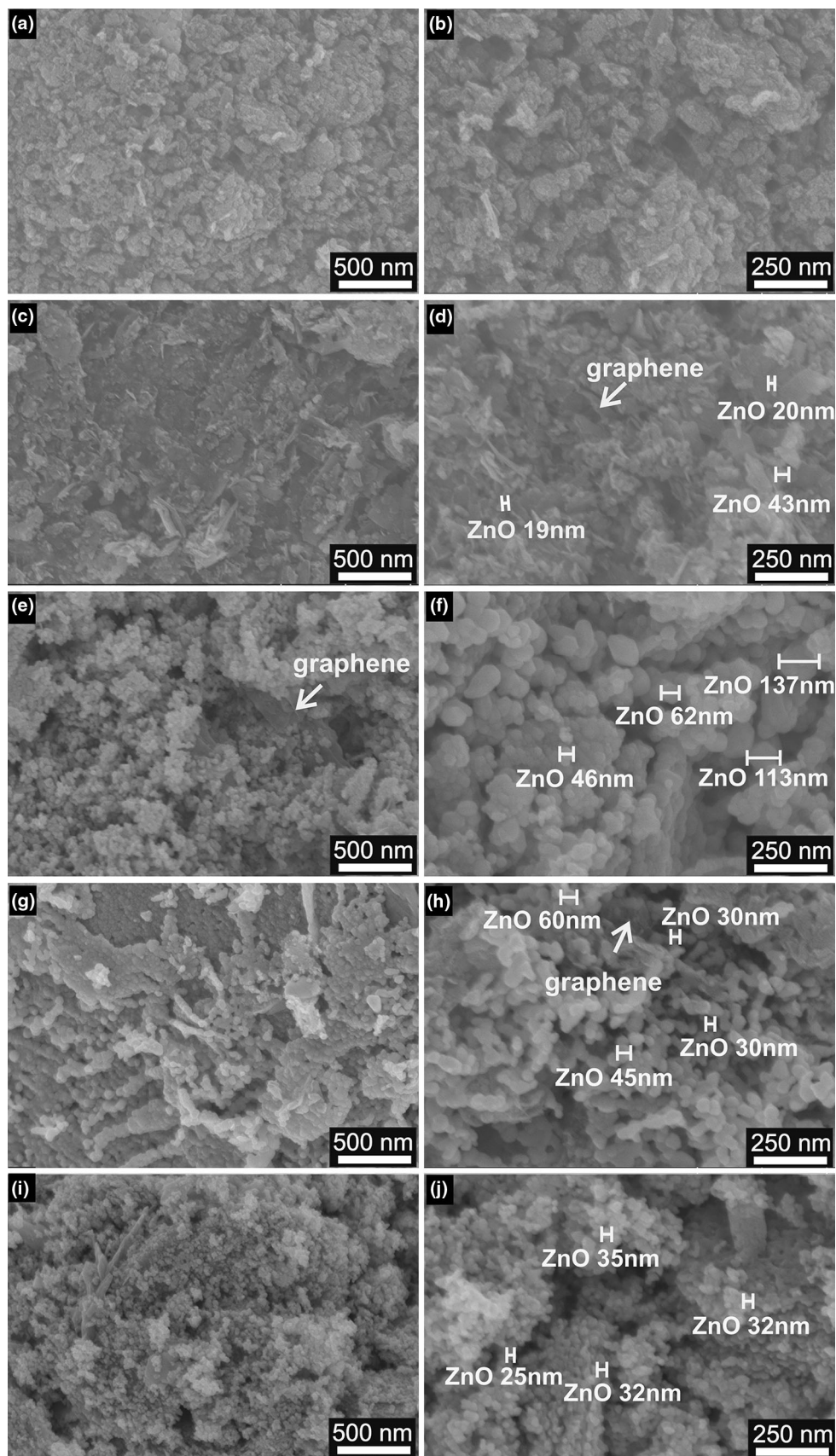


Fig. 5. (a, b) Scanning electron microscopy (SEM) images of pure rGO. Graphene–ZnO nanocomposites with ratios of (c, d) 3:1, (e, f) 1:1, and (g, h) 1:3. (i, j) Pure ZnO.

via van der Waals interactions, making it very difficult to see the sheets on SEM images, although sheet edges can occasionally be seen. In graphene–ZnO with 3:1 composition (Fig. 5c and d) edges of rGO sheets were visible. On the surface of the rGO sheets, very small ZnO particles were formed, but their size could not be confirmed from the SEM image. ZnO particles with size ranging from 50 nm to 137 nm started to be visible at the 1:1 composition (Fig. 5e and f). The presence of ZnO nanoparticles became clearer at graphene:ZnO ratio of 1:3, as shown in Fig. 5g and h. Nanoparticles with size ranging from 30 nm to 60 nm were attached to the surface of rGO. The size of the ZnO particles at this ratio was smaller than the ZnO observed for the graphene–ZnO nanocomposite with ratio of 1:1, indicating that the rGO concentration strongly affected the size and distribution of ZnO. This phenomenon can be explained as follows: For the graphene–ZnO composite with 1:1 ratio, rGO was plentiful enough to permit self-nucleation and thus with the ZnO. Self-nucleation of ZnO made the particles become bigger. At the 1:3 ratio, ZnO and rGO prevented self-nucleation of each other and made their distribution quite uniform and the ZnO particles smaller. Furthermore, from Fig. 5i and j,

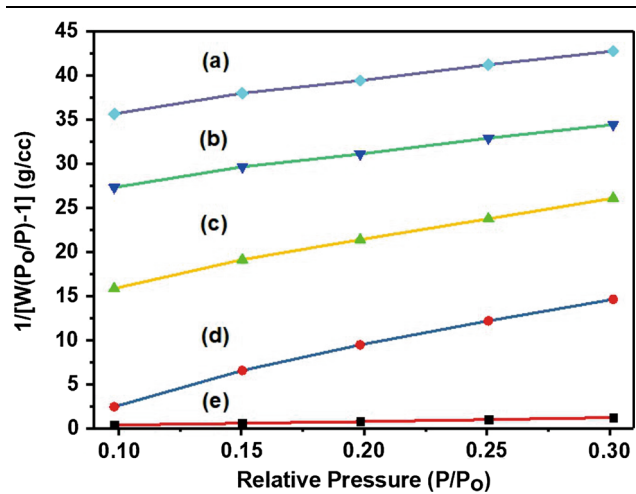


Fig. 6. (a) BET surface area as function of relative pressure for rGO. GZ nanocomposites with ratios of (b) 3:1, (c) 1:1, and (d) 1:3. (e) ZnO.

we conclude that the ZnO in the composite had the same circular shape as the pure ZnO.

Based on the SEM results, we can also describe the process that occurred while refluxing. The reflux process of zinc nitrate tetrahydrate in ethylene glycol results in formation of zinc glycolate. The aging process for 12 h would cause zinc glycolate particles to settle on the surface of the sheets as well as in the spaces between the rGO sheets. Furthermore, the calcination process would cause the zinc glycolate to decompose into ZnO particles, formed on the surface of the rGO and between sheets of rGO. ZnO that formed between rGO sheets increased the distance between them, and conversely the size of the ZnO was restricted by the distance between the rGO sheets.

The results of nitrogen adsorption–desorption measurements on the five samples are shown in Fig. 6, while the BET calculation results for the specific surface area are presented in Table II, together with the atomic percentages calculated from energy-dispersive spectroscopy (EDS) analysis (Fig. 7).

Based on the BET calculation, the specific surface area of rGO and ZnO was 844 m²/g and 53 m²/g, respectively. The high specific surface area of rGO could increase the specific surface area of the graphene–ZnO composites. As a result, the higher the concentration of rGO in the composite, the higher its specific surface area. Presence of rGO in the composite could increase the specific surface area from 53 m²/g to 94 m²/g. EDS analysis of rGO resulted in a C:O ratio of 155:1, a good value compared with many results.¹⁹ The number of oxygen atoms in the composites was higher than the number of zinc atoms, possibly because the reflux and calcination processes caused some rGO sheets to be oxidized. The Zn:O ratio in pure ZnO indicates presence of oxygen vacancies, confirming the *n*-type semiconductor nature of ZnO.

The data obtained from the sensor characterization are plotted as the dynamic response of the sensor. The change in the response on exposure to the target gas was calculated using Eq. 4, where R_a is the resistance before exposure and R_g is the resistance with the target gas flowing through the chamber. This response change is usually called the response sensitivity, hence the term sensitivity is used here. Besides the sensitivity, we also

Table II. Specific surface area and EDS results for all samples

Sample	rGO	GZ 3:1	GZ 1:1	GZ 1:3	ZnO
Specific surface area (m ² /g)	844	94	67	76	53
EDS (at.%)					
C	99.4	46.77	47.86	23.03	–
O	0.64	42.21	38.15	62.21	34.62
Zn	–	11.02	13.99	14.76	65.38

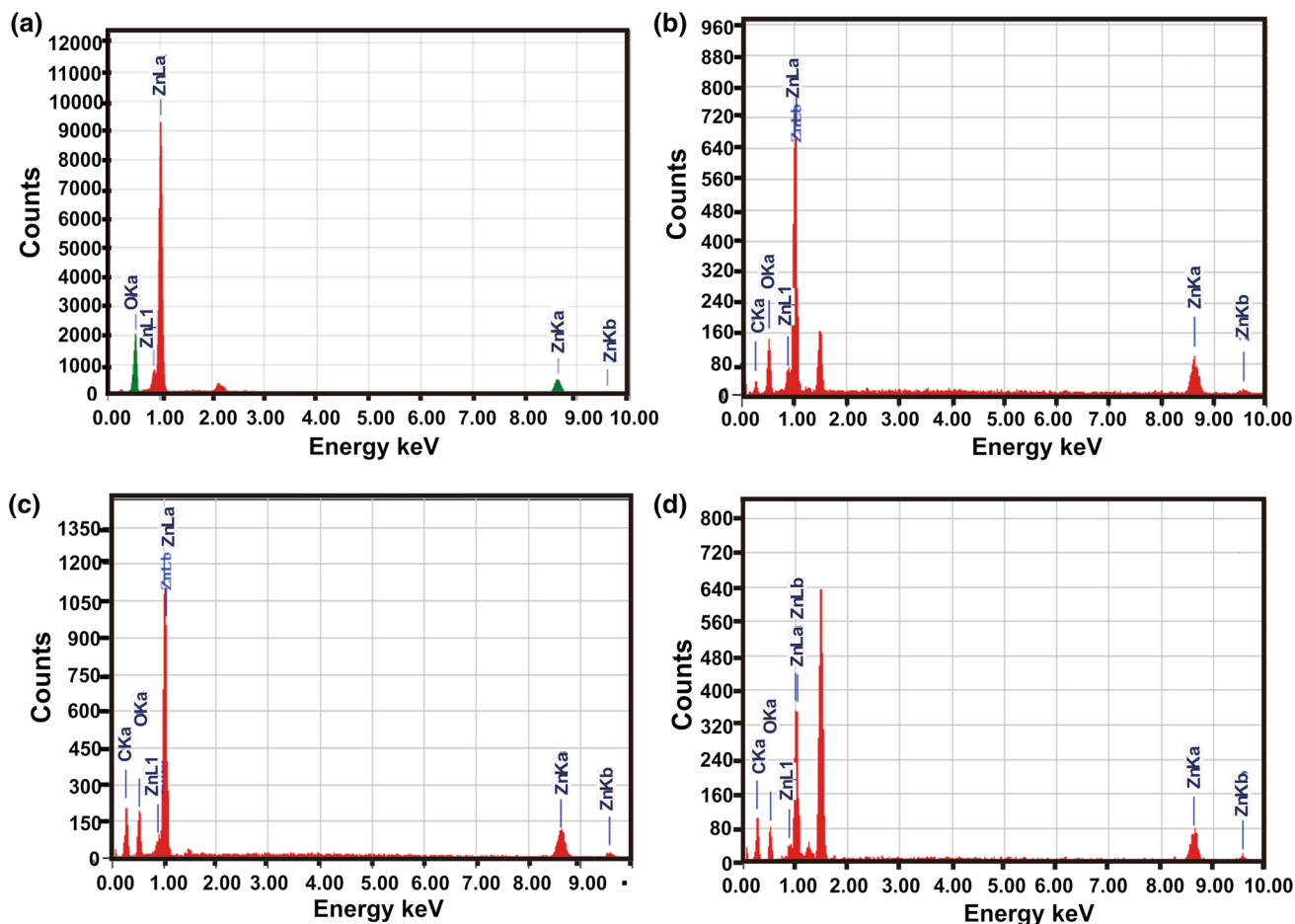


Fig. 7. Energy-dispersive spectra of (a) ZnO, (b) GZ 1:3, (c) GZ 1:1, and (d) GZ 1:3.

calculated the response and recovery times, i.e., the time needed for the sensor to reach 90% of its steady-state value.

$$\Delta R(\%) = \frac{R_a - R_g}{R_a} \times 100. \quad (4)$$

Each sample was tested using 30 ppm CO in the temperature range from 25°C to 300°C. The dynamic response of the sensor for all samples is shown in Fig. 8. As discussed above, the samples were all semiconductors. All sensors except one (the pure rGO sensor at room temperature) showed a positive response, i.e., the resistance decreased when exposed to the target gas. CO is a reducing gas and will cause a decrease of the resistance for an *n*-type semiconductor sensor.

At room temperature, pure rGO acts as a *p*-type semiconductor, whose resistance will increase on interaction with CO. However, at high temperature, the resistance of rGO decreased on interaction with CO. This *p*-type semiconductor response of rGO at room temperature is in agreement with some

previous reports,^{12,20–23} proving that graphene acts as a *p*-type semiconductor at room temperature. The negative response of rGO at room temperature and the positive response at higher temperatures indicate a change in semiconductor type, from *p*- to *n*-type, as the temperature was increased. Normally, rGO acts as a *p*-type semiconductor with holes as major charge carriers.^{24,25} This change at high temperature indicates a change in the charge carrier. In the case of the composites, all samples showed *n*-type behavior, with resistance that decreased on exposure to CO gas. This phenomenon indicates that the sensors followed the behavior of ZnO, with graphene resulting in enhanced conductivity and gas adsorption.²⁶ In the sensing process, similar to pure ZnO, oxygen ionsorption on the ZnO surface plays an important role. In ambient atmosphere, oxygen adsorbs on the ZnO surface, ionizes to form O[−] by taking an electron from the conduction band, and creates a depletion layer. The interaction between CO and O[−] will form CO₂ and release an electron back to the conduction band, leading to a decrease in resistance. Furthermore, presence of CO could also alter the barrier potential

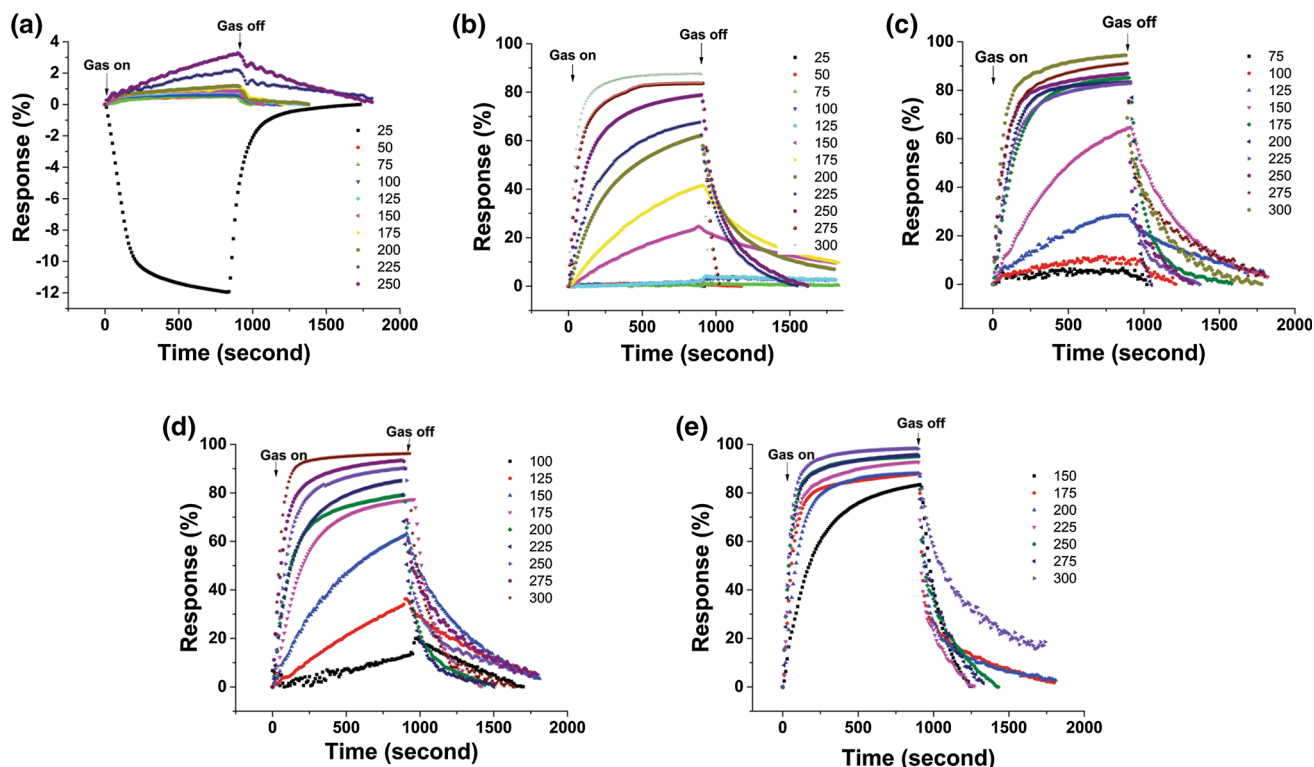


Fig. 8. Dynamic response of GZ nanocomposite sensors with ratios of (a) 1:0, (b) 3:1, (c) 1:1, (d) 1:3, and (e) 0:1 on exposure to 30 ppm CO at different temperatures.

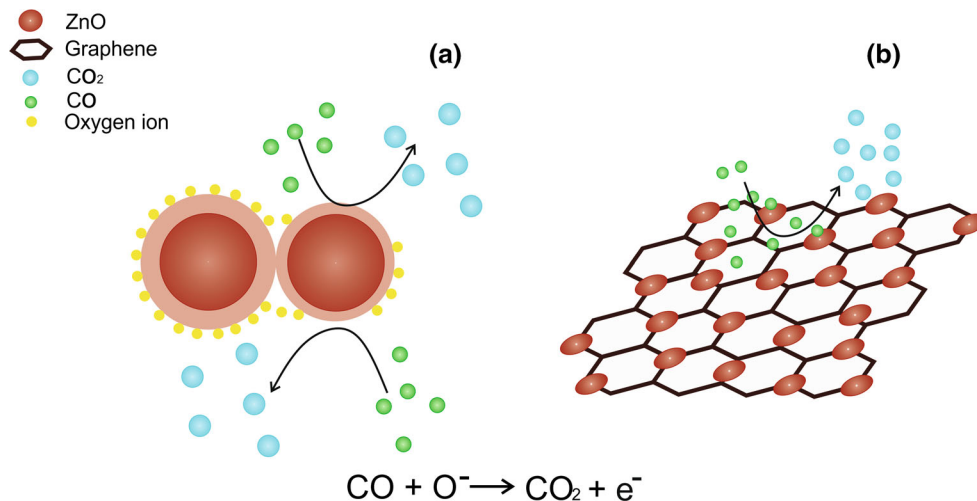


Fig. 9. (a) Schematic of sensing mechanism of pure ZnO and (b) graphene-ZnO nanocomposite sensors.

at the rGO-ZnO interface, also contributing to the sensing mechanism. A schematic comparing the sensing mechanisms is shown in Fig. 9.

The temperature dependence of the response of the graphene-ZnO nanocomposite sensors is shown in Fig. 10. For all samples, the sensor response increased as the operating temperature was increased. High temperature gives the target gas sufficient energy to overcome the activation energy for surface reaction, hence the higher the

temperature, the higher the response. Furthermore, the graphene-ZnO nanocomposites showed a response at low temperatures below 150°C, while pure ZnO only started to show a response at 150°C. It was observed that the minimum operating temperature of the graphene-ZnO nanocomposite sensors with ratio of 3:1, 1:1, and 1:3 was 25°C (room temperature), 75°C, and 100°C, respectively, clearly lower than the value of 150°C for pure ZnO. These results clearly prove that addition of graphene to

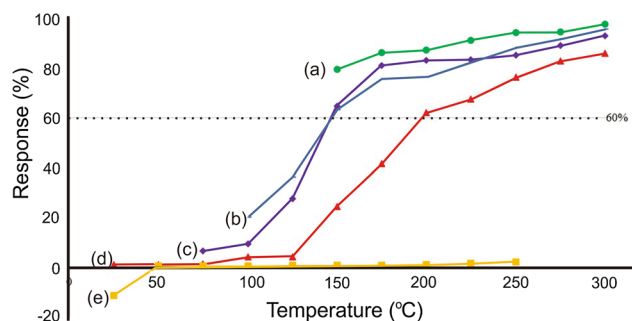


Fig. 10. Sensor response of (a) ZnO, (b) GZ 1:3, (c) GZ 1:1, (d) GZ 3:1, (e) rGO as function of operating temperature in the range of 25°C to 300°C.

ZnO can decrease the operating temperature of sensors to the low-temperature region between room temperature and 125°C. Moreover, sensitivity above 60% was observed at operating temperature of 150°C for the graphene–ZnO nanocomposite with ratio of 1:1 or 1:3. In the range of 175°C to 300°C, the response of the graphene–ZnO composites with ratio of 1:1 and 1:3 followed the pattern for ZnO but showed lower sensitivity.

To the best of the authors’ knowledge, to date, there is no research on synthesis of graphene–zinc oxide by reflux technique for CO gas sensors. The results presented herein are competitive with other works on different types of material for CO gas sensing, or with similar materials for sensing of different gases, as well as similar materials and techniques for other gases, as summarized in Table III. The developed nanocomposites can detect CO gas well at concentration of 30 ppm, lower than most other studies, where the CO concentration was above 100 ppm. Moreover, the sensor also showed good CO gas sensing response at 150°C, while other sensors mostly showed good CO gas sensing performance at temperatures above 300°C. This comparison indicates that the presented nanocomposite sensor has high potential to detect low CO concentration well at low temperature.

CONCLUSIONS

The reflux technique proved to be a simple and low-cost method to synthesize graphene–ZnO nanocomposite films. The rGO–ZnO composites exhibited CO gas sensing in the range from room temperature to 125°C, lower than for pure ZnO. In this low-temperature region, the graphene–ZnO nanocomposite with ratio of 1:3 exhibited the highest sensor response, followed by those with ratio of 1:1 and 3:1, which showed the lowest response among the composites. The performance of the graphene–ZnO nanocomposites in this low operating temperature region is much better than that of pure ZnO. Pure ZnO started to show sensor response at operating temperature of 150°C. Although pure ZnO showed the highest sensitivity at high temperature above 150°C among

Table III. Comparison of carbon monoxide gas sensors

Sensing material	Method	Target gas concentration (ppm)	Response (%)	Temperature (°C)	Ref.
SnO ₂	Spray pyrolysis	CO (200)	~ 50	375	27
Al-doped ZnO	Microemulsion	CO (100)	60	350	28
In ₂ O ₃	Electrospinning	CO (100)	550	300	29
GdInO ₃ and reduced-graphene-decorated GdInO ₃	Solvothermal	CO (100)	75	200	30
WO ₃	Sol-gel	CO (250)	40	100	31
Sm ₂ O ₃	Coprecipitation	CO (4000)	~ 19	400	32
Pd-loaded SnO ₂ /PrGO	Hydrothermal	CO (50–1600)	1–9.5	26	33
Graphene–ZnO	Microwave irradiation	CO (10)	45	300	34
Graphene–ZnO	Thermal reduction	NH ₃ (50)	~ 3	Room temperature	35
Graphene–ZnO	Modified carbothermal reduction	NH ₃ (50)	19.2	Room temperature	36
Graphene–ZnO	Reflux technique	H ₂ (200)	75	150	37
Graphene–ZnO	Reflux technique	CO (30)	36	125	This work
			98	300	

all the samples, the graphene–ZnO composites showed sensitivity not far below that of pure ZnO. Moreover, addition of rGO to ZnO did not affect the response time, while the recovery time was observed to be improved.

ACKNOWLEDGEMENTS

This work has been partly supported by Research Grant of Research, Technology, and Higher Education Ministry, World Class Professor Program (WCP) Research, Technology, and Higher Education Ministry and Research Grant of Research Group Institut Teknologi Bandung.

REFERENCES

- H. Mustafic, P. Jabre, C. Caussin, M.H. Murad, S. Escolano, M. Tafflet, M.-C. Perier, E. Marijon, D. Vernerey, J.-P. Empana, and X. Jouven, *JAMA* 307, 713 (2012).
- M. Vrijheid, D. Martinez, I. Aguilera, M. Bustamante, F. Ballester, M. Estarlich, A.F. Somoano, M. Guxens, N. Lertxundi, M.D. Martinez, A. Tardon, and J. Sunyer, *Epidemiology* 23, 23 (2012).
- R.J. Levy, *Carbon Monoxide Anesth.* 123, 670 (2016).
- K.R. Amin and A. Bid, *Curr. Sci.* 107, 430 (2014).
- F. Schedin, A. Geim, S. Morozov, E. Hill, P. Blake, M. Katsnelson, and K. Novoselov, *Nat. Mater.* 6, 652 (2007).
- C.A. Betty, *Mater. Sci. Technol.* 32, 375 (2016).
- B. Yulianto, M.F. Ramadhani, Nugraha, N.L.W. Septiani, and K.A. Hamam, *J. Mater. Sci.* 52, 4543 (2017).
- N.L.W. Septiani, B. Yulianto, Nugraha, and H.K. Dipojono, *Appl. Phys. A* 123, 1 (2017).
- B. Yulianto, L. Nulhakim, M.F. Ramadhani, M. Iqbal, S. Nugraha, and A. Nuruddin, *IEEE Sensors J.* 15, 4114 (2015).
- H.J. Yoon, D.H. Jun, J.H. Yang, Z. Zhou, S.S. Yang, and M.M.-C. Cheng, *Sensors Actuators B* 157, 310 (2011).
- H. Jayatissa, *Solid State Electron.* 2012, 159 (2012).
- K. Anand, O. Singh, and R.C. Singh, *Appl. Phys. A* 116, 1141 (2014).
- S. Liu, B. Yu, H. Zhang, T. Fei, and T. Zhang, *Sensors Actuators B* 202, 272 (2014).
- R.K. Joshi, Q. Hu, F. Alvi, N. Joshi, and A. Kumar, *J. Phys. Chem.* 113, 16199 (2009).
- G. Singh, A. Choudhary, D. Haranath, A.G. Joshi, N. Singh, S. Singh, and R. Pasricha, *Carbon* 50, 385 (2012).
- X. Liu, L. Pan, Q. Zhao, T. Lv, G. Zhu, T. Chen, T. Lu, Z. Sun, and C. Sun, *Chem. Eng. J.* 183, 238 (2012).
- K.L. Foo, U. Hashim, K. Muhammad, and C.H. Voon, *Nanoscale Res. Lett.* 9, 429 (2014).
- M. Nasrollahzadeh, B. Jaleh, and A. Jabbari, *RSC Adv.* 4, 36713 (2014).
- S. Pei and H.-M. Cheng, *Carbon* 50, 3210 (2012).
- G. Lu, L.E. Ocola, and J. Chen, *Appl. Phys. Lett.* 94, 083111-1 (2009).
- J.D. Fowler, M.J. Allen, V.C. Tung, Y. Yang, R.B. Kaner, and B.H. Weiller, *ACS Nano* 3, 301 (2009).
- M. Qazi, T. Vogt, and G. Koley, *Appl. Phys. Lett.* 91, 233101-1 (2007).
- D.-T. Phan and G.-S. Chung, *J. Phys. Chem. Solids* 74, 1509 (2013).
- C.I.L. Justino, A.R. Gomes, A.C. Freitas, A.C. Duarte, and T.A.P. Rocha-Santos, *TrAC Trends Anal. Chem.* 91, 53 (2017).
- S.S. Varghese, S. Lonkar, K.K. Singh, S. Swaminathann, and A. Abdala, *Sensors Actuators B* 218, 160 (2015).
- F.-L. Meng, Z. Guo, and X.-J. Huang, *TrAC Trends Anal. Chem.* 68, 37 (2015).
- E. Lackner, J. Krainer, R.W. Teubenbacher, F. Sosada, M. Deluca, C. Gspan, K. Rohrer, E. Wachmann, and A. Kock, *Mater. Today Proc.* 4, 7128 (2017).
- S.K. Lim, S.H. Hong, S.-H. Hwang, W.M. Choi, S. Kim, H. Park, and M.G. Jeong, *J. Mater. Sci. Technol.* 31, 639 (2015).
- S.K. Lim, S.-H. Hwang, D. Chang, and S. Kim, *Sensors Actuators B* 149, 28 (2010).
- C. Balamurugan, S. Arunkumar, and D.-W. Lee, *Sensors Actuators B* 234, 155 (2016).
- D. Susanti, A.S. Perdana, H. Purwaningsih, L. Noerochim, and G.E. Kusuma, *AIP Conf. Proc.* 1586, 14 (2014).
- C.R. Michel, A.H. Martinez-Preciado, R. Parra, C.M. Aldao, and M.A. Ponce, *Sensors Actuators B* 202, 1220 (2014).
- M. Shojaee, Sh. Nasresfahani, and M.H. Sheikhi, *Sensors Actuators B* 254, 457 (2018).
- H.W. Kim, Y.J. Kwon, A. Mirzaei, S.Y. Kang, M.S. Choi, J.H. Bang, and S.S. Kim, *Sensors Actuators B* 249, 590 (2017).
- H. Tai, Z. Yuan, W. Zheng, Z. Ye, C. Liu, and X. Du, *Nanoscale Res. Lett.* 11, 130 (2016).
- T. Wang, Z. Sun, D. Huang, Z. Yang, Q. Ji, N. Hu, G. Yin, D. He, H. Wei, and Y. Zhang, *Sensors Actuators B* 252, 284 (2017).
- K. Anand, O. Singh, M.P. Singh, J. Kaur, and R.C. Singh, *Sensors Actuators B* 195, 409 (2014).